ME-85-02

Effect of Slag Cement on Corrosion

B.B. Hope
A.K. Ip
D.G. Manning

Ontario

Ministry of
Transportation and
Communications

Research and
Development
Branch

86-04025/

Technical Report Documentation Page

MTC Report Number ME-85-02	ISBN Number	Other Document Number	Date Nov 1985

Title: Effect of Slag Cement on Corrosion

Authors: **Brian B. Hope,** Professor
Alan K. Ip, Research Associate

Department of Civil Engineering
Queen's University at Kingston

David G. Manning
Head, Materials & Engineering Systems Research
Research & Development Branch, MTC

Published by:

The Research and Development Branch
Ontario Ministry of
Transportation & Communications

Abstract:
This investigation examines the effect of slag cement on corrosion of embedded reinforcing steel. Both microcell and macrocell corrosion were included in the study.

In the microcell corrosion study, a total of 18 reinforced slabs made with concrete containing different proportions of slag and Portland cement were subjected to various wetting and drying cycles. The corrosion currents in the slabs were determined using the linear polarization method. The results showed that the corrosion rates of steel embedded in the slabs decreased with increasing slag content except during the first few days after casting. This was mainly caused by the gain in the electrical resistivity of the concrete, which increased with increase in slag content after the initial curing. The resistivity of concrete made with slag cement appeared to be more susceptible to a change in storage condition.

In the macrocell corrosion study, three typical reinforced slabs were mortared to cathode blocks which were made with Portland cement and contained a relatively large quantity of steel. It was found the macrocell corrosion currents dropped rapidly after the anode and cathode were electrically coupled and became steady in about a day. The magnitudes of the corrosion currents at the steady state were small in all the specimens.

Key Words: corrosion, slag cement, cathodic protection

Comments: Prepared for the 65th Annual Meeting of the Transportation Research Board, Washington, D.C.

Distribution: Unrestricted, corrosion engineers and those involved with bridge design and rehabilitation

Copyright Status: Crown copyright

ME-85-02

Effect of Slag Cement on Corrosion

B.B. Hope
Professor, Department of Civil Engineering
Queen's University at Kingston

A.K. Ip
Research Associate, Department of Civil Engineering
Queen's University at Kingston

D.G. Manning
Head, Materials and Engineering Systems Research
Research and Development Branch, MTC

Published by:
The Research and Development Branch
Ontario Ministry of Transportation and Communications
Hon. Ed Fulton, Minister
D.G. Hobbs, Deputy Minister

Published without prejudice
as to the applications of the findings.
Crown copyright reserved; however, this
document may be reproduced for non-commercial
purposes with attribution to the Ministry.

For additional copies write:
The Editor, Technical Publications
Ministry of Transportation and Communications
Room 320, Central Building
1201 Wilson Avenue
Downsview, Ontario
Canada M3M 1J8
(416) 248-7226

September 1985

NOTATION

η	overpotential
β_a	anodic Tafel slope
β_b	cathodic Tafel slope
i_o	corrosion current
R_p	polarization resistance
I	applied current
CM	corrosion rate
M	equivalent weight
F	Faraday
CMD	corrosion rate density
A	surface area of corroded electrode
ρ_c	concrete electrical resistivity
R_c	concrete electrical resistance
E_o	corrosion potential
δE	anode/cathode potential difference
T	absolute temperature

TABLE OF CONTENTS

1. INTRODUCTION 1

2. SLAG CEMENT

2.1 Granulated Slag 1
2.2 Portland Blast-Furnace Slag Cement 2

3. CORROSION

3.1 Chloride Diffusion 3
3.2 Corrosion Resistance of Slag Cement 3

4. MEASUREMENT TECHNIQUES

4.1 Corrosion Measurement 4
4.2 Concrete Electrical Resistivity Measurement 6
4.3 Temperature Effect 6

5. EXPERIMENTAL WORK

5.1 Specimens 7
5.2 Corrosion Measurement 8
5.3 Concrete Electrical Resistivity Measurement 9
5.4 Visual Assessment of Embedded Steel 9
5.5 Chloride Content 9

6. RESULTS AND DISCUSSION

6.1 General 9
6.2 Microcell Specimens 10
6.3 Visual Assessment of Embedded Steel 12
6.4 Chloride Content 12
6.5 Macrocell Specimens 12

7. CONCLUSIONS 13

REFERENCES 14

LIST OF TABLES

Table		
1.	Chemical analysis of the slag and Portland cements	17
2.	Properties of the fine and coarse aggregates	17
3.	Mix design for the concrete	18
4.	Test slabs for microcell measurement	18
5.	Storage conditions for the microcell test slabs	19
6.	Visual assessment of corrosion of the embedded steel	20
7.	Water soluble chloride content of the concrete samples	21

LIST OF FIGURES

Figure		
1.	A typical slab for microcell measurement	22
2.	Cathode steel	22
3.	Cathode block	23
4.	A typical mortared slab	23
5.	Concrete resistivity, steel potential, and corrosion current in a typical slab made with 100% Portland cement	24
6.	Concrete resistivity, steel potential, and corrosion current in a typical slab made with 75% Portland and 25% slag cement	25
7.	Concrete resistivity, steel potential, and corrosion current in a typical slab made with 50% Portland and 50% slag cement	26
8.	Average concrete resistivity, steel potential, and corrosion current in the oven dried slabs made with 100% Portland cement	27
9.	Average concrete resistivity, steel potential, and corrosion current in the oven dried slabs made with 75% Portland and 25% slag cement	28
10.	Average concrete resistivity, steel potential, and corrosion current in the oven dried slabs made with 50% Portland and 50% slag cement	29
11.	Relationship between corrosion rate and concrete electrical resistivity	30
12.	Corrosion on typical bars embedded in the slabs made with 100% Portland cement	31
13.	Corrosion on typical bars embedded in the slabs made with 75% Portland and 25% slag cement	31

14. Corrosion on typical bars embedded in the slabs made with 50% Portland and 50% slag cement 32

15. Macrocell corrosion current in a typical mortared slab 33

1. INTRODUCTION

In 1980 the Ontario Ministry of Transportation and Communications used a blend of Portland and blast furnace slag cement in a bridge deck on a trial basis for the first time. The Ministry permits the use of blended cement in non-structural concrete but requires further evaluation before its use for structural concrete can be approved.

It is known that some blended cements have reduced calcium hydroxide compared with Portland cement and this causes a reduction in pH of the concrete. The protection afforded to reinforcing steel against corrosion results from the high pH of Portland cement concrete. Consequently, the Ministry was concerned that the reduced pH of blended cement may permit corrosion of the reinforcing steel under conditions where no corrosion would occur in Portland cement concrete.

This study was initiated to determine whether the use of blended cement will likely affect the corrosion of steel in concrete. The results of the study will permit the Ministry to develop a policy for the use of blended blast furnace slag cement in structural concrete. The use of such a cement could lead to a reduced cost of concrete.

2. SLAG CEMENT

2.1 Granulated Slag

Blast-furnace slag is a by-product from the reduction of iron ore in the manufacture of pig iron. It is composed of lime, silica, and alumina, with minor amounts of magnesia, iron oxide and alkali oxides (the same oxides that make up Portland cement, but not in same proportions). After molten slag is rapidly chilled or quenched in water, it solidifies as a glass. This glassy product is known as granulated slag.

In the presence of suitable ctivators, such as calcium hydroxide and calcium sulfate, all except the more silicious granulated slags show marked cementitious properties (1). Generally, the hydraulic properties of granulated slags depend upon chemical composition, fineness, and degree of vitrification achieved during rapid chilling.

2.2 Portland Blast-Furnace Slag Cement

Portland blast-furnace slag cement is a type of hydraulic cement consisting of a blend of Portland cement and fine granulated slag of selected quality.

The heat evolution during the setting and hardening of slag cement varies with the composition of both the Portland cement clinker and of the granulated slag, as well as with their relative properties. During the hydration process, the Portland cement component hydrates initially in the normal manner. The calcium hydroxide formed during the hydration of the Portland cement then activates the granulated slag. They form new compounds of lower solubility and greater stability. The identified hydration products in set slag cements are (1):

1. A tobermorite-like calcium silicate hydrate phase.

2. Hexagonal tetracalcium aluminate hydrate or its solid solution.

3. An ettringite-type phase.

4. Calcium hydroxide.

The amount of calcium hydroxide present in the set slag cement varies with the Portland cement to slag ratio. The alkaline nature of the hydrated calcium silicates in slag cement paste is somewhat less than that in Portland cement. Von and Efes (3) reported that the pH of hydrated slag cement pastes which had been hydrated up to one year was in the range of 12.

Because slags react slowly during hydration, the hydration rate of slag cement is relatively slow and comparable to modified Portland cement (CSA Type 20).

Slag cement paste has a more compact structure than Portland cement paste. The proportion of the pores being smaller than 30 nm in the cement paste increases with increasing slag content (3).

Pore structure of the slag cement paste is affected by storage condition. The cement paste would become more porous when stored in sodium chloride or calcium chloride solution (3,4). The pore structure also appears to depend upon the fineness of the cement. Mikhail and co-workers (4) found that the porosity was lower in the pore structure of the slag cement of higher Blaine area.

3. CORROSION

3.1 Chloride Diffusion

Corrosion of steel embedded in an aqueous medium is not likely to occur if the pH of the medium is between 8 to 13 as the steel is either immune or passivated (5). Since the pH of the uncarbonated concrete is approximately 12.5, the embedded steel is normally protected from corrosion.

The intrusion of chloride ions in reinforced concrete can destroy the passivity of the embedded steel and corrosion would proceed if oxygen and moisture were also available to support the corrosion reaction.

Chloride can permeate through hardened concrete and the chloride diffusion depends upon concrete cover, water/cement ratio and cement type.

Studies (3,6,7) found that chloride penetration decreased with decreasing water/cement ratio and increasing depth of concrete.

Test results (3,8,9) showed that the chloride diffusion into mortar and concrete specimens made with slag cement was lower compared with specimens made with Portland cement and the diffusion rate decreased with increase in slag content of the cement. The decrease of diffusion rate of chloride is probably due to the more compact pore structure of the slag cement paste and the relatively high C_3A content. Gjørv and Vennesland (9) suggest the diffusion rate of chloride in concrete also depends on the exchange of anions between the permeating salt solution and the pore solution of the concrete. For slag cement, the capacity for exchanging anions with the permeating solution is lower because of the lower concentration of hydroxyl ions in the pore solution.

3.2 Corrosion Resistance of Slag Cement

A number of studies have been conducted on corrosion of steel in slag cement concrete and Portland cement concrete (3,10-13).

Von and Kfes (3) found that the steel bars embedded in slag cement concretes showed less corrosion than those in Portland cement concretes. The test specimens had been exposed to various cycles of wetting (soaking in NaCl solution) and drying (storing in air).

Mather (12) indicated that the embedded steel in the slag cement concretes showed less corrosion compared to the ASTM Type 2 Portland cement concretes after the specimens had been moist cured in the laboratory for 90 days.

Ost and Monfore (13), however, found that there was no difference in the susceptibility to corrosion of prestressing wires in the slag cement concrete and Portland cement concretes.

Gouda and co-workers (10,11) indicated that the corrosion resistance was appreciably affected by the degree of fineness of the slag cement. In the slag cement pastes produced from high Blaine area cement, the behaviour of embedded steel was similar to that in the Portland cement pastes. The corrosion resistance of the slag cement paste increased with increasing fineness of the slag cement.

4. MEASUREMENT TECHNIQUES

4.1 Corrosion Measurement

4.1.1 Microcell and Macrocell Corrosion

Two types of corrosion cells: microcell and macrocell, may exist in a bridge deck. The microcell is characterized by small distance separation of the anode and cathode. In such a cell, only the mixed potential at the anode and cathode can be measured. In macrocell corrosion, the anodic and cathodic reactions frequently take place in areas located some distance apart and the potentials of the anode and cathode are known. In laboratory study, the corrosion currents in both types of cells can be measured using appropriate methods.

4.1.2 Microcell Corrosion Measurement

Different techniques described in the literature (14-20) can be used to determine the corrosion current in a microcell. Among those methods, the linear polarization method developed by Stern and Geary (14) shows the most reliable result in determining the corrosion rate of single steel embedded in concrete (21).

Stern and Geary consider the slope of the overpotential of a corroded specimen versus the applied current (I) for small values of the overpotential (η). This slope, $d\eta/dI$, referred to as polarization resistance, is related to the corrosion current, i_o, by the expression:

$$\frac{d\eta}{dI} = \frac{1}{2.3\, i_o} \left(\frac{\beta_a \beta_c}{\beta_a + \beta_c} \right) = \frac{B}{i_o} \qquad (1)$$

where

β_a = anodic Tafel slope

β_c = cathodic Tafel slope

Escalante et al (21) found from comparison of gravimetric weight loss measurements of corroding steel bars in chloride-contaminated concrete that values of $\beta_a = \beta_c = 100$ mV were appropriate. These Tafel slopes yield a value of 21.7 for the constant B. Gonzalez et al (22), also using weight loss data, concluded that the values for B are 26 and 52 for steel in the active and passive states, respectively. For this study all the linear polarization measurements have been reduced to corrosion currents using a value of 21.7 for B so that, after rearranging, Equation 1 becomes:

$$i_o = \frac{21.7}{R_p} \quad mA \qquad (2)$$

where $R_p = d\eta/dI$ (ohms)

Once the corrosion current is known, the corresponding corrosion rate can be determined by Faraday's Laws. The first and second of Faraday's Laws imply that the corrosion rate in a corrosion system is directly proportional to corrosion current. In equation form, the corrosion rate, CM, can be expressed as:

$$CM = i_o\left(\frac{M}{F}\right) \qquad (3)$$

where i_o = corrosion current

M = equivalent weight

F = Faraday (96,487 Coulombs/equivalent weight)

Noting equivalent weight of Fe^{2+} ion is 27.93 grams, the corrosion rate per unit area, CMD, may be given by:

$$CMD = 0.00913\left(\frac{i_o}{A}\right) \quad g/cm^2yr \qquad (4)$$

where A = surface area of corroded electrode in cm^2

4.1.3 Macrocell Corrosion Measurement

The polarization method of corrosion measurement described in Section 4.1.2 is not applicable for determination of the corrosion currents in macrocells (23). In this situation, the corrosion current flow between anode and cathode can only be determined by direct measurement. Since it is not possible to measure current directly, current values are obtained by measuring voltage drop across a resistor incorporated in the circuit.

4.2 Concrete Electrical Resistivity Measurement

Electrical resistivity of a particular reinforced concrete test specimen cannot be calculated directly from electrical resistance measured between the embedded steel because of the unknown path length and cross-sectional area. A calibration factor is required in order to convert the measured resistance to resistivity. The method used to obtain this constant is given in Reference 24. Firstly, all the embedded steel, which is arranged in the exact pattern used for each slab, is placed in a solution of known resistivity. The electrical resistance between each electrode pair is then recorded. The calibration factor is equal to the known resistivity of the solution divided by the measured resistance. The resistivity of any test slab is obtained by multiplying the resistance reading between the electrodes by the calibration factor.

4.3 Temperature Effect

Concrete electrical resistivity changes with change in temperature. Consequently, corrosion current is affected by the temperature change. The relationship between temperature, concrete electrical resistivity, and corrosion current are given below.

Based on Hinrichson-Rasch Law, the relationship between resistivity and temperature may be expressed by:

$$\rho_{c1} = \rho_{c2}\, e^{a\left(\frac{1}{T_1} - \frac{1}{T_2}\right)} \qquad (5)$$

where ρ_{c1} = resistivity at temperature T_1

ρ_{c2} = resistivity at temperature T_2

a = constant

T_1 and T_2 are in degrees absolute

Equation 5 can be used to estimate electrical resistivity of a concrete specimen at a selected temperature if its resistivity at a reference temperature is known. The value of 'a' was found to be in the range from 2130 to 2880 (24-26).

The relation between corrosion current and temperature is developed using Ohm's Law and based on the assumption that the driving circuit voltage in a corrosion cell will remain constant when the resistance of the system changes instantaneously:

$$i_{o1} = \frac{i_{o2}}{e^{a\left(\frac{1}{T_1} - \frac{1}{T_2}\right)}} \qquad (6)$$

where i_{o1} = corrosion current at temperature T_1

i_{o2} = corrosion current at temperature T_2

'a', T_1, and T_2 are the same as in Equation 5

Clear (24) indicates that the underlying assumption that circuit voltage remains constant is basically accurate within an error range of 5% which is considered acceptable.

5. EXPERIMENTAL WORK

5.1 Specimens

5.1.1 Concrete

Two types of commercial cements (Type 10, normal Portland cement; and Type 10S, Portland blast-furnace slag cement) were used for this investigation. The chemical composition of these cements are listed in Table 1. The properties of the aggregates and mix design for the concrete are shown in Tables 2 and 3.

5.1.2 Microcell Slabs

The test specimens were 113 x 300 x 400 mm slabs. Three 13 mm smooth mild steel bars were embedded 250 mm in concrete and centred at 56 mm from the top surface of each slab. The bar located at the centre of the slab was used as a counter electrode and the other two bars, placed 144 mm on each side of the centre bar, were active electrodes. All the bars were used as received and no attempt was made to remove the mill scale. The protruding ends of the bars at the concrete surfaces were sealed with either wax or plastic tubes and silicon.

Three batches of concrete were made with 100% normal Portland cement (batch A), 75% normal Portland cement and 25% Portland blast-furnace slag cement (batch B), and 50% normal Portland cement and 50% Portland blast-furnace slag cement (batch C). Six slabs were cast from each batch. The data on the specimens are summarized in Table 4 and a typical slab is shown in Figure 1.

5.1.3 Cathode Blocks

The specimens were 113 x 300 x 400 mm reinforced slabs made with normal Portland cement. The embedded steel in each block was composed of three 13 mm smooth mild steel bars and two 3 x 75 x 200 mm mild steel plates (Figure 2). The total steel surface area was 87500 mm^2. A typical cathode block is shown in Figure 3.

5.1.4 Storage and Testing Schedule

After demoulding, Slab series A, B, and C were cured in water for 36, 34, and 35 days, respectively. All the slabs were then subjected to various cycles of wetting (immersed in a 3.5% sodium chloride solution) and drying (stored in laboratory air) as given in Table 5.

For Slabs A1, B1, and C1, the initial steel corrosion and concrete electrical resistance readings were taken at the 7th day, and the subsequent readings were taken starting with the 13th, 11th, and 12th days, respectively. For the remainder of the slabs, steel corrosion and concrete electrical resistance readings were taken every 7 days starting with the 7th day.

At a later stage, the following tests were performed:

1. Two slabs from each series were oven dried at 105°C for 14 days. The slabs were soaked in air saturated water for the next 14 days and dried in laboratory air for the following 14 days. Steel corrosion and concrete electrical resistance measurements were taken starting with the second day of soaking.

2. Three typical slabs from the series were mortared to the surfaces of the cathode blocks. These mortared slabs were used to determine the instantaneous transient and steady state corrosion current flow from anode to cathode. The specimens were stored in laboratory air followed by ponding with water. Steel corrosion and concrete electrical resistance measurements were taken before and after the pond. A typical specimen is shown in Figure 4.

5.2 Corrosion Measurement

5.2.1 Microcell Corrosion Measurement

During testing, the corrosion potentials of the test bars in the slab series A to C were initially counterbalanced by a commercial potentiostat. Each bar was then polarized by 4 mV and 8 mV overpotentials for 1 ms from a signal generator. The corresponding potential pulse outputs were recorded on the screen of an oscilloscope and were converted into currents afterwards. The slope of the plot

of the applied overpotentials versus the currents was equal to R_p in Equation 2.

5.2.2 Macrocell Corrosion Measurement

For each of the mortared slabs, the transitory corrosion current flow from the anode to cathode was monitored from the time of connection of the anode to cathode for up to several days by measuring the potential drop across a 50-ohm resistor incorporated in the connection between the anode and cathode and the results recorded on an x-y plotter. The steady state current flow was determined by measuring the potential drop across the 50-ohm resistor using a voltmeter capable of reading to an accuracy of 1μV.

5.3 Concrete Electrical Resistivity Measurement

The electrical resistance of concrete between the bars was measured by a commercial digital impedance meter. Sodium bromide solution was used in the determination of the resistivity calibration factor. The measured resistance multiplied by a factor of approximately 19 is the corresponding resistivity in ohm-cm.

5.4 Visual Assessment of Embedded Steel

At the end of the test period, three slabs from each series were cut open using a diamond saw. A visual assessment of the corrosion of the embedded steel bars was then performed. The corrosion of the bars was indicated using a rust index ranging from 1 for very slight or no corrosion to 4 for relatively heavy corrosion.

5.5 Chloride Content

After bars had been cut from slabs described in Section 5.4, concrete prisms were cut from the middle portion of one slab from each series. Water soluble chloride contents were determined for six sections of each prism taken from the slab surface to the bar centre line. The six sections were 10 mm centre to centre and were ground to facilitate chloride extraction.

6. RESULTS AND DISCUSSION

6.1 General

A summary of the test results is shown in Tables 6 and 7 and Figures 5 to 15.

The effects of various storage conditions on the average concrete electrical resistivities, steel electrical potentials, and corrosion currents in slab series A to C are shown in Figures 5 to 10. All the corrosion current and

concrete electrical resistivity data in the figures are not adjusted to a reference temperature. The range of temperature during the test period was from 19 to 22°C and most readings were taken at about 21°C. All the concrete resistivity data are 1 kHz readings and the corrosion currents are obtained from Equation 2.

The influence of concrete electrical resistivity on the corrosion current is shown in Figure 11.

The rust formations on the bars from the typical slabs are shown in Figures 12 to 14. The assessment of the corrosion of the bars is recorded in Table 6.

Table 7 shows the water soluble chloride content of the concrete samples.

Figure 15 shows the macrocell corrosion current in a typical mortared slab. The current data on the right portion of the graph were taken when the anode and cathode were electrically connected momentarily.

6.2 Microcell Specimens

6.2.1 Concrete Electrical Resistivity

The average concrete electrical resistivity for series C slabs, made with 50% slag and 50% Portland cement, was found to be the lowest at the 7th day. At the later stage, however, the average concrete electrical resistivity of the slabs increased with increasing slag content.

After 7 days of curing, for concretes B (made with 25% slag and 75% Portland cement) and C (made with 50% slag and 50% Portland cement), the gain in resistivity with age was relatively quick compared to concrete A (made with 100% Portland cement). For example, the average concrete resistivity readings for the slab series B and C were about 110% and 75% of that for the slab series A. They were about 175% and 300% of the latter at the later stages. This may be due to the following cause: The conduction of electrical current in moist concrete is essentially electrolytic in nature, hence, the electrical resistivity of concrete will be controlled by the alkali salt content of the evaporable water in the capillary pores of the cement paste. Since the pore structure is more compact and the hydration products are less basic in slag cement paste than those in Portland cement paste, the resistivity of concrete increases with increase in slag content. The initial slow gain in concrete resistivity of slab series C was due to the relatively slow hydration rate.

The concrete resistivity for the slab series C appeared to be affected by the various drying and wetting cycles to a larger extent than series A or B as shown from Figures 5 to 7.

After the oven dried slabs were soaked in water, the concrete resistivity decreased rapidly. The lowest values of the resistivity ranged from about 2500 ohm-cm for slab series A to 5000 ohm-cm for slab series C, and were about 5 to 8 times less than they were before the slabs were oven dried.

6.2.2 Steel Potential

The steel potentials in all the slabs were in the range from -400 mV to -600 mV CSE in the first 14 days. They decreased rapidly in the remaining curing period.

After the slabs were subjected to the first wetting and drying cycle, the steel potentials increased steadily. When the slabs were subjected to the 3 day/3 day and 3 day/11 day wetting and drying cycles, they varied from -300 mV to -500 mV CSE.

After the oven dried slabs were soaked in water, the steel potentials in the slabs increased markedly. They were in the range from -400 mV to -600 mV CSE.

6.2.3 Corrosion Current

The average corrosion current in slab series B was the lowest at the 7th day. At the later stages, the corrosion current decreased with increasing slag content. For instance, at the 124th day, the average corrosion current in slab series C was approximately 55% and 35% of those in slab series B and A, respectively.

For all the slabs, the corrosion currents decreased with age up to about 60 days after the wetting and drying cycles had been started.

For the oven dried slabs, the corrosion currents reached their peak values at about 20 days after the soaking was commenced. The range of these maximum values was from 490 μA in slab series C to 910 μA in slab series A. The high corrosion current likely results from the low concrete resistivity and large amount of oxygen diffused into the system.

From the test data, it is quite clear that the electrical resistivity of concrete can give good indications of corrosion rate of steel if the other parameters necessary for corrosion, such as oxygen and depassivation, are present. Under a given storage condition the corrosion rate of a corroding steel embedded in a concrete can be predicted if the resistivity of the concrete is known. For example, Figure 11 may be used to estimate the corrosion rates of the steel samples in the slabs, which were alternately dried in air and soaked in salt solution, regardless of the concrete mix proportions.

6.3 Visual Assessment of Embedded Steel

Examination of the embedded steel bars showed that:

- The rust on most of the bars concentrated in the area below the concrete surface at the protruding end of the steel (Table 6 and Figures 12 to 14).

- The heaviest corrosion occurred on the bars embedded in the slabs which were oven dried followed by soaking in water.

- The average corrosion of the bars embedded in the slabs made with Portland cement was heavier than that of the bars embedded in the slabs made with slag cement and Portland cement.

6.4 Chloride Content

The water soluble chloride contents of the samples described in Section 5.5 are given in Table 7. Each value represents only one sample from one slab and should not, therefore, be considered accurate average values. They do show clearly, however, that the chlorides had penetrated to the level of the reinforcing steel over the testing duration. In addition, the chloride diffusion generally decreased with increasing slag cement content and increasing depth of concrete.

6.5 Macrocell Specimens

In all the mortared slabs, the corrosion current flows dropped rapidly after the anode and cathode steel were electrically coupled (Figure 15). The magnitudes of the current flows in the test specimens decreased 6- to 7-fold after one day. This drop in current was mainly caused by the polarization of the steel or depletion of available oxygen or both. After this initial drop, the corrosion current flow became quite steady. When the anode and cathode were disconnected, the potential differences increased rapidly and tended to return to the initial value in about one day.

All the three macrocell corrosion cells indicated small steady corrosion current flow. The corrosion current increased about 2 times after the specimens were ponded with water. This was probably caused by the decreased resistivities of the concretes.

It appears that the major controlling factors of the macrocell corrosion are the resistivity of the concrete, availability of oxygen for cathodic reaction, and the differential concentration of the corrosion cells (e.g., chloride to choride free cells).

7. CONCLUSIONS

The results of this investigation indicated that:

1. Corrosion of the steel embedded in the mature microcell slabs decreased with increasing slag cement content. This was accompanied by a corresponding higher concrete electrical resistivity and lower chloride diffusion rate.

2. Corrosion of the steel embedded in the microcell slabs was dependent on the nature of the storage condition. The corrosion rates increased dramatically after the concretes were completely dried followed by soaking in water.

3. Under similar conditions of chloride ion and oxygen availability, corrosion rates of the steel embedded in the microcell slabs were a direct function of concrete electrical resistivity, regardless of the concrete mix components.

4. Electrical resistivity of concrete made with slag cement was more susceptible to a change in storage condition. Consequently, the corrosion rate of steel embedded in such a concrete may be influenced by the ambient conditions to a larger extent compared to that in Portland cement concrete.

5. Macrocell corrosion currents in the mortared slabs dropped rapidly after the anode and cathode were electrically connected and reached steady state in about a day. The magnitude of the currents at the steady state were small in all the slabs.

REFERENCES

(1) Lea, F.M., "The Chemistry of Cement and Concrete," 3rd Edition, Edward Arnold Publishing, U.K., 1970, pp.454-489.

(2) Malhotra, V.M., "Strength and Freeze-Thaw Characteristics of Concrete Incorporating Granulated Blast-Furnace Slag," Division Report 79-38, CANMET, Energy, Mines and Resources Canada, 1979.

(3) Von Dr.-Ing, and Yakut Efes, "Effect of Cements with Varying Content of Granulated Blast-Furnace Slag on Chloride Diffusion in Concrete," Betonwerk+Fertigteil - Technik, Heft 4/80, pp. 224-229, 5/80, pp.302-306, and 6/80, pp. 365-368.

(4) Mikhail, R. Sh., Mourad, W.E., and Gouda,V.K., "Hardened Portland Blast-Furnace Slag Cement Pastes: I. Effects of Additives on Surface Area and on Pore Structure," Cement and Concrete Research, Vol. 4, No. 5, 1974, pp.807-820.

(5) Pourbaix, M., Atlas of Electrochemical Equilibrium in Aqueous Solutions, Pergamon Press Limited, London, 1976.

(6) Ost, B., and Monfore, G.E., "Penetration of Chloride into Concrete," Journal of the PCA Research Development Laboratory, Jan. 1966, pp. 46-52.

(7) Clear, K.C., "Time-to-Corrosion of Reinforcing Steel in Concrete Slabs, vol. 3, Performance after 830 Daily Salt Applications," Report No. FHWA-RD-76-70, Federal Highway Administration, Washington, D.C., 1976, 64 pp.

(8) Gjørv, O. E., and Vennesland, O., "Diffusion of Chloride Ions from Seawater into Concrete," Cement and Concrete Research, Vol. 9, No. 2, 1979, pp. 229-238.

(9) Collepardi, M., Marcialis, A., and Turriziani, R., "Penetration of Chloride Ions into Cement Pastes," Journal of American Ceramic Society, Vol. 55, 1972, pp. 534.

(10) Gouda, V. K., Shater, M.A., and Mikhail, R.Sh., "Hardened Portland Blast-Furnace Slag Cement Pastes: II. The Corrosion Behavior of Steel Reinforcement," Cement and Concrete Research, Vol. 5, No. 1, 1975, pp. 1-13.

(11) Gouda, V. K., Mikhail, R. Sh., and Shater, M. A., "Hardened Portland Blast-Furnace Slag Cement Pastes: III. Corrosion of Steel Reinforcement Versus Pore Structure of The Paste Matrix," Cement and Concrete Research, Vol. 5, No. 2, 1975, pp. 99-102.

(12) Mather, B., "Laboratory Tests of Portland Blast-Furnace Slag Cements," ACI Journal, Proceedings Vol.54, Sept. 1957, pp. 205-232.

(13) Ost, B., and Monfore, G.E., "Corrodibility of Prestressing Wire in Concretes Made With Type 1 and Type 15 Cements," PCA Journal, May 1963, pp. 23-26.

(14) Stern and Geary, "A Theoretical Analysis of the Shape of Polarization Curves," Journal of Electrochemical Society, Vol. 104, No. 1, 1957, pp. 56-63.

(15) Holler, H.D., "Studies on Galvanic Couples: II. Some Potential-Current Relations in Galvanic Corrosion," Journal of the Electrochemical Society, Vol. 97, No. 9, 1950, pp. 277282.

(16) Schwerdtfeger, W.J., and McDorman, O.N., "Measurement of the Corrosion Rate of a Metal from its Polarizing Characteristics," Journal of the Electrochemical Society, Vol. 99, No. 10, 1952, pp. 407-413.

(17) Barnartt, S., "Two-Point and Three-Point Methods for the Investigation of Electrode Reaction Mechanisms," Electrochimica Acta, Vol. 15, 1970, pp. 1313-1324.

(18) Mansfeld, F., "Tafel Slopes and Corrosion Rates from Polarization Resistance Measurements," Corrosion, NACE, Vol. 29, No. 10, Oct. 1973, pp. 397-402.

(19) Mansfeld, F., "Polarization Resistance Measurements Experimental Procedure and Evaluation of Test Data," Electrochemical Techniques for Corrosion, NACE, 1977, pp. 18-26.

(20) Dean, Jr., S.W., "Electrochemical Methods of Corrosion Testing," Electrochemical Techniques for Corrosion, NACE, 1977, pp. 52-60.

(21) Escalante, E., Ito, S., and Cohen, M., "Measuring the Rate of Corrosion of Reinforcing Steel in Concrete," National Bureau of Standards, NBSIR 80-2012, Mar. 1980.

(22) Gonzalez, J.A., Algaba, S., and Andrade, C.," Corrosion of Reinforcing Bars in Carbonated Concrete," British Corrosion Journal, Vol.15, No.3, 1980, pp.135-139.

(23) Slater, J.E., "Corrosion on Metals in Association with Concrete," MPC Project 880-2, The Metal Properties Council, N.Y., 1981, 142 pp.

(24) Clear, K.C., "Cost Effective Rigid Concrete Construction and Rehabilitation in Adverse Environments," FCF Annual Progress Report, Project No. 4K, 1981.

(25) Whittington, H.W., McCarter, J., and Forde M.C., "Resistivity Characteristics of Concrete," Proceeding of Institute Civil Engineers, Vol. 71, Part 2, Mar. 1981, pp. 107-117.

(26) "Electrical Impedance of Concrete." M.T.C. Report, Project No. 22120, 1982.

Table 1. Chemical analysis of the slag and Portland cements

Chemical analysis :	Slag %	Portland cement
CaO	38.79	63.19
SiO_2	39.37	20.91
MgO	12.65	2.64
Al_2O_3	7.19	5.81
SO_3	1.54	3.00
MnO	0.69	-
Fe_2O_3	0.52	2.12
K_2O	-	1.26
TiO_2	0.29	-

Table 2. Properties of the fine and coarse aggregates

Aggregate type	Maximum size (mm)	Bulk density	Fineness Modulus	Absorption (%)
Fine	-	2.67	2.64	0.8
Coarse	19	2.68	3.20	0.6

Table 3. Mix design for the concrete

Cement	CSA Type 10 or/and CSA type 10S
Fine aggregage	natural siliceous sand
Coarse aggregate	crushed limestone aggregate
Mixing water	tap water
Cement content	400 kg/m^3
Cement/aggregate/water	1.00/4.25/0.45
Slump	75 ± 25 mm
Air content	6 ± 1 %
Admixtures	water reducing agent Pozzolith 83 air entraining agent MB-AE 10

Table 4. Test slabs for microcell measurement

Slab no.	Cement type	Active electrode surface area (mm^2)
A1 - A6	100% Portland	10250
B1 - B6	75% Portland;25% slag	10250
C1 - C6	50% Portland;50% slag	10250

Table 5: Storage conditions for the microcell test slabs

Slab no.	Curing period	Age (days) Wetting and drying periods* 1-hr daily ponding	1-day soaking 1-day drying	3-day soaking 3-day drying	3-day soaking 11-day drying
A1	1 - 36	37 - 68	69 - 88	89 - 116	117 - 194
B1	1 - 34	35 - 66	67 - 86	87 - 114	115 - 192
C1	1 - 35	36 - 67	68 - 87	88 - 115	116 - 193
A2-A6	1 - 36	37 - 68	69 - 88	89 - 116	117 - 124
B2-B6	1 - 34	35 - 66	67 - 86	87 - 114	115 - 123
C2-C6	1 - 35	36 - 67	68 - 87	88 - 115	116 - 123

*Wetting in a 3.5% NaCl solution and drying in laboratory air

Table 6. Visual assessment of corrosion of the embedded steel

Slab	Bar no.	Rust index	Maximum depth (mm)*	Comment
A1	1	1	15	
	3	2	25	
A4+	10	4	55	rust area concentrated on one side
	12	3	50	a rust spot located on the other end
A5+	13	3	35	
	15	3	30	a rust spot located on the other end
B1	1	1	20	
	3	1	15	
B4+	10	3	40	
	12	2	30	
B5+	13	2	30	
	15	3	35	
C1	1	2	20	
	3	1	15	
C4+	10	3	55	narrow strip rust area
	12	2	25	a rust spot at 40 mm from the other end
C5+	13	3	45	
	15	4	60	

* The depth was measured from the concrete surface at the protruding end of the steel

+ Oven dried slabs

Table 7. Water soluble choride content of the concrete samples

Slab	Sample	Distance from concrete surface	Chloride content
A	1	0 - 10	0.270
	2	10 - 20	0.180
	3	20 - 30	0.174
	4	30 - 40	0.141
	5	40 - 50	0.097
	6	50 - 60	0.066
B	1	0 - 10	0.228
	2	10 - 20	0.206
	3	20 - 30	0.181
	4	30 - 40	0.111
	5	40 - 50	0.091
	6	50 - 60	0.060
C	1	0 - 10	0.211
	2	10 - 20	0.172
	3	20 - 30	0.132
	4	30 - 40	0.097
	5	40 - 50	0.071
	6	50 - 60	0.049

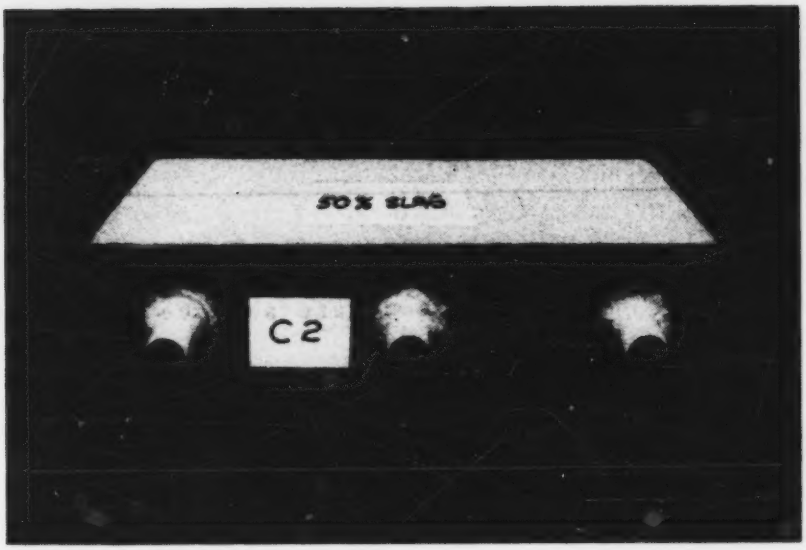

Fig. 1. A typical slab for microcell measurement

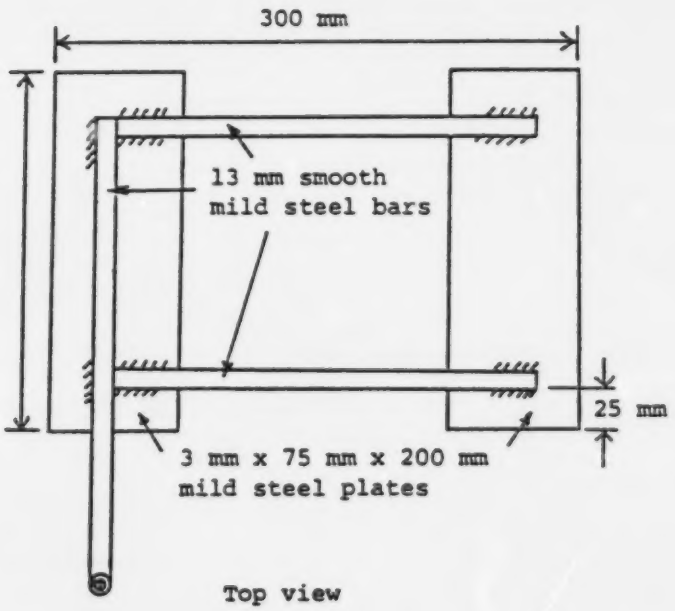

Fig. 2. Cathode steel

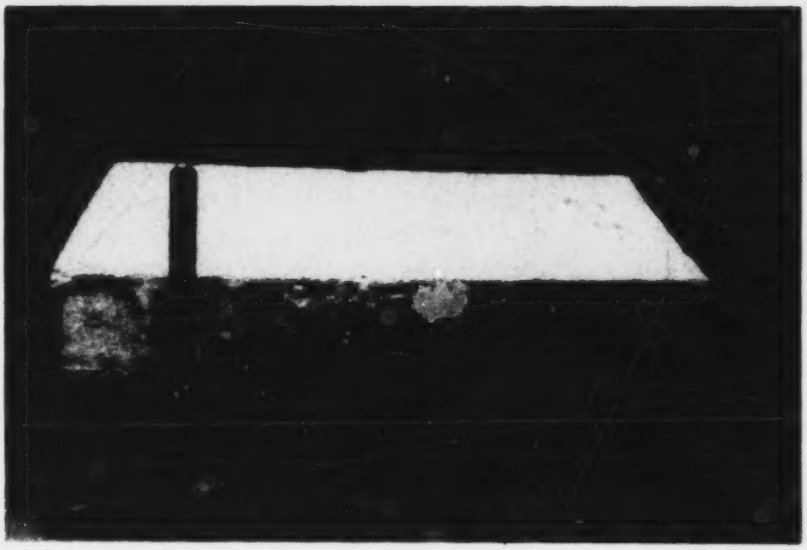

Fig. 3. Cathode block

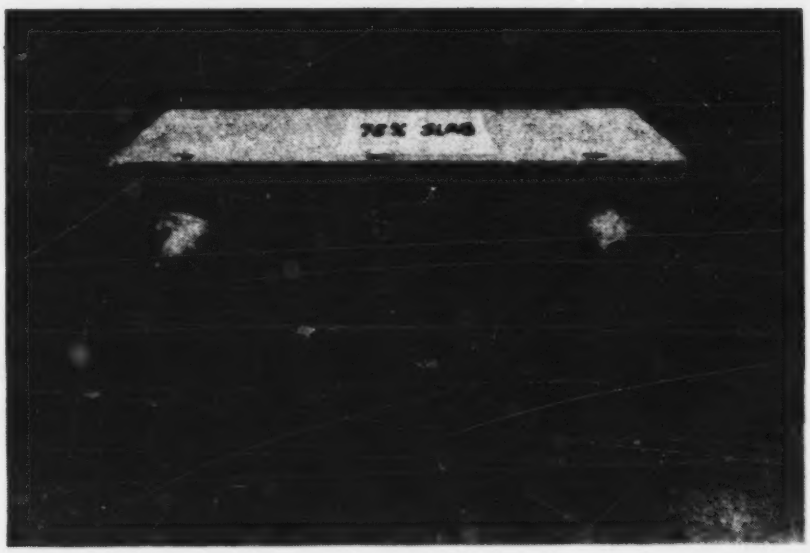

Fig. 4. A typical mortared slab

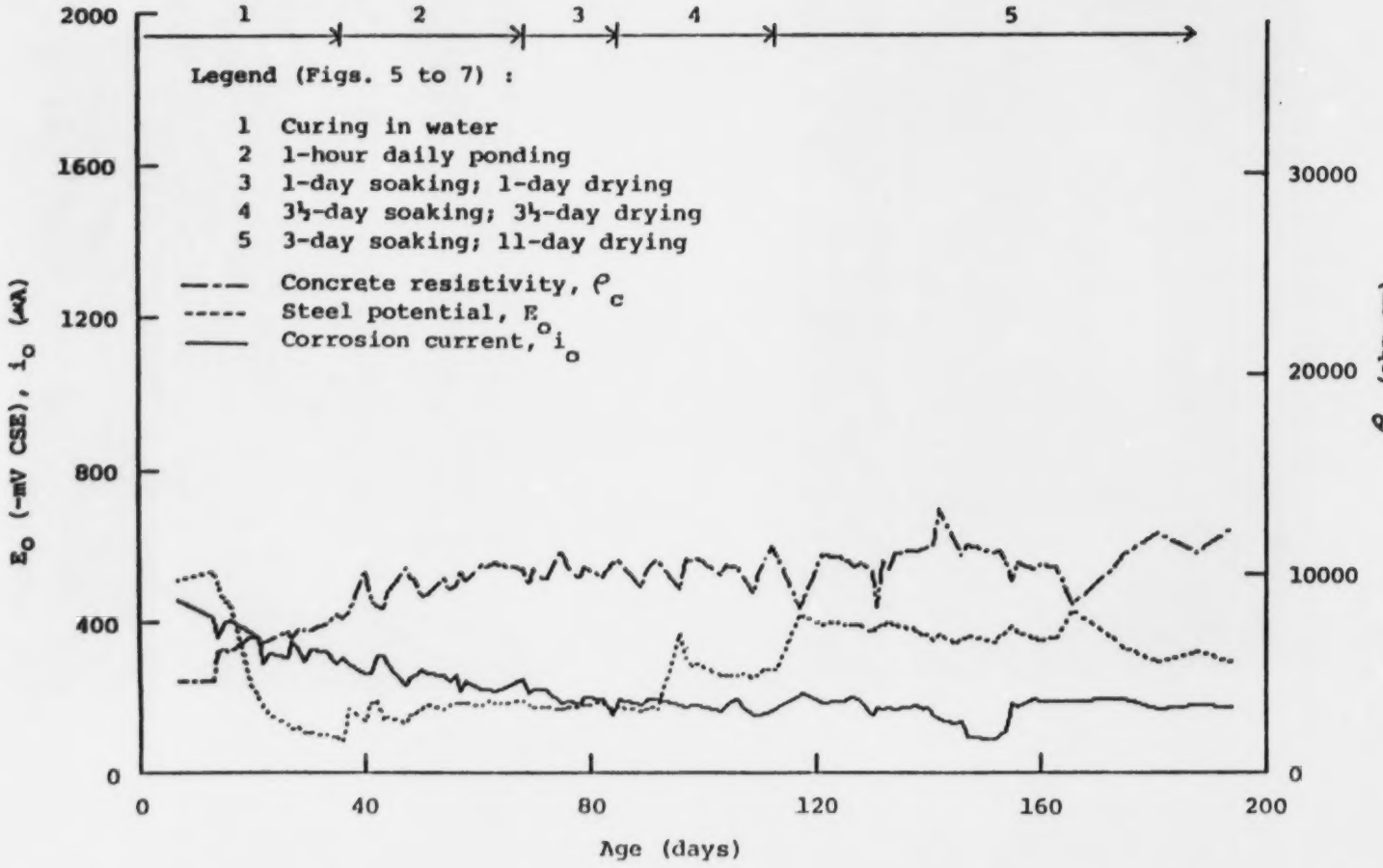

Fig. 5. Concrete resistivity, steel potential, and corrosion current in a typical slab made with 100 % Portland cement

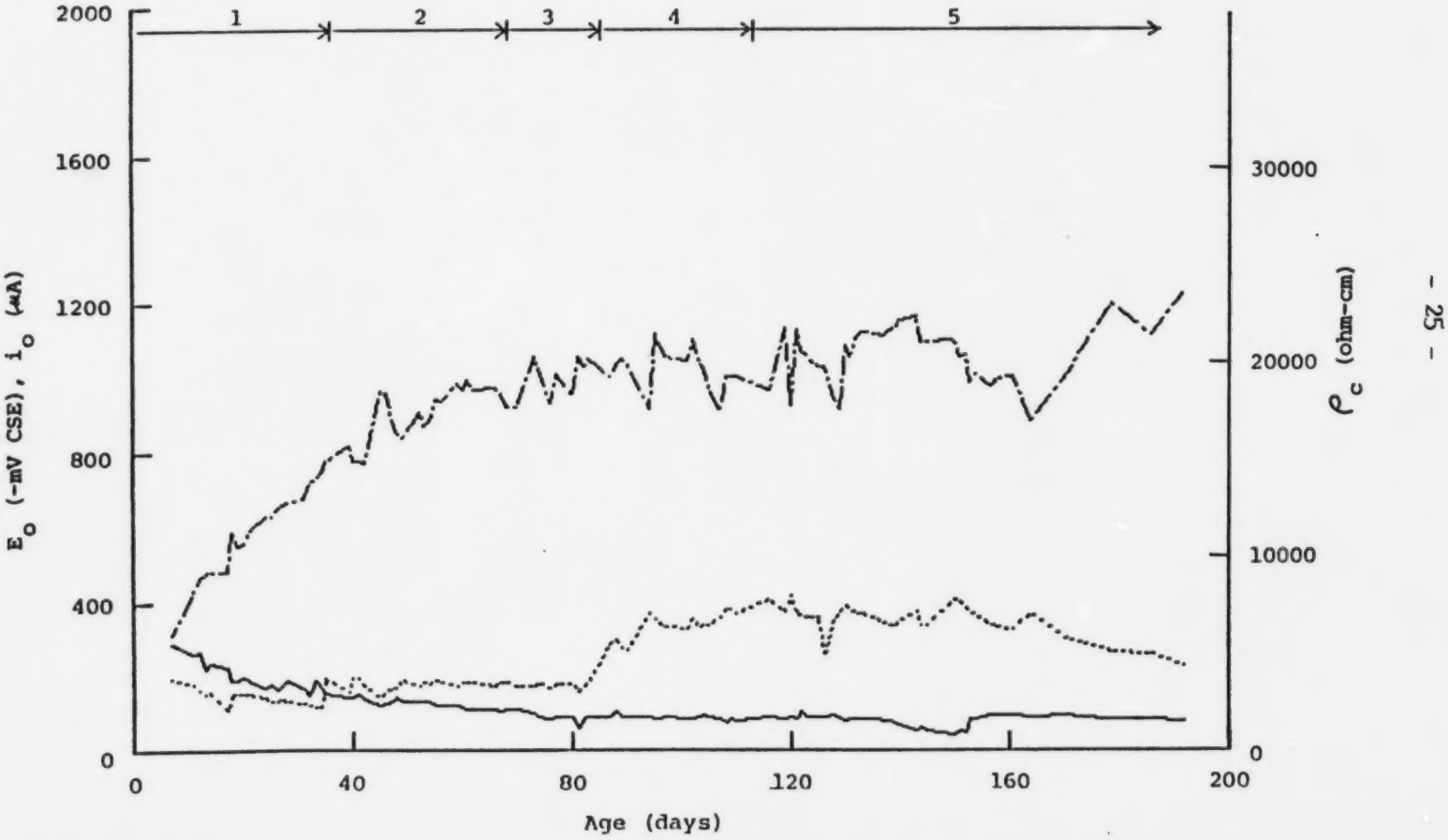

Fig. 6. Concrete resistivity, steel potential, and corrosion current in a typical slab made with 75 % Portland and 25 % slag cement

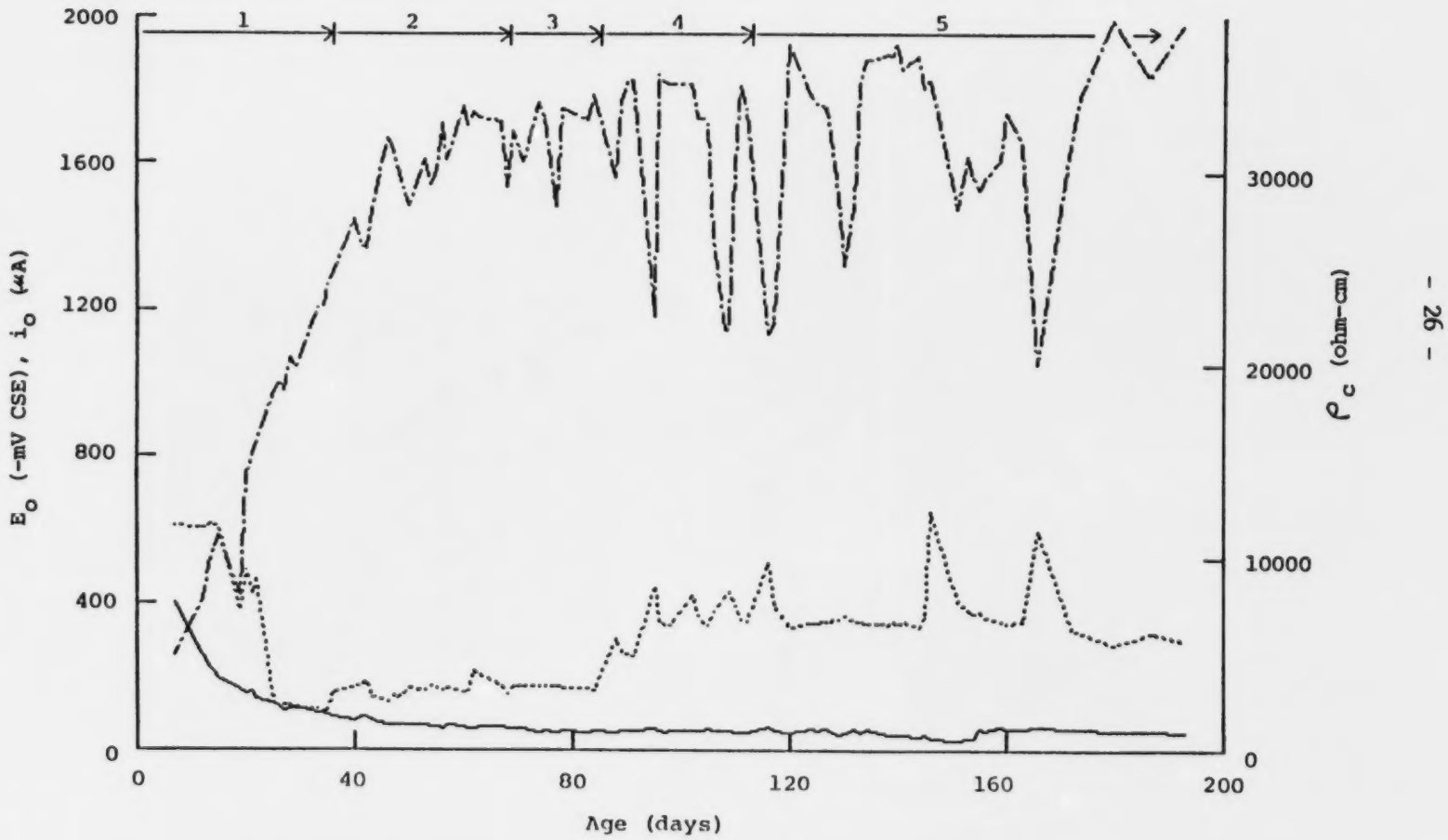

Fig. 7. Concrete resistivity, steel potential, and corrosion current in a typical slab made with 50 % Portland and 50 % slag cement

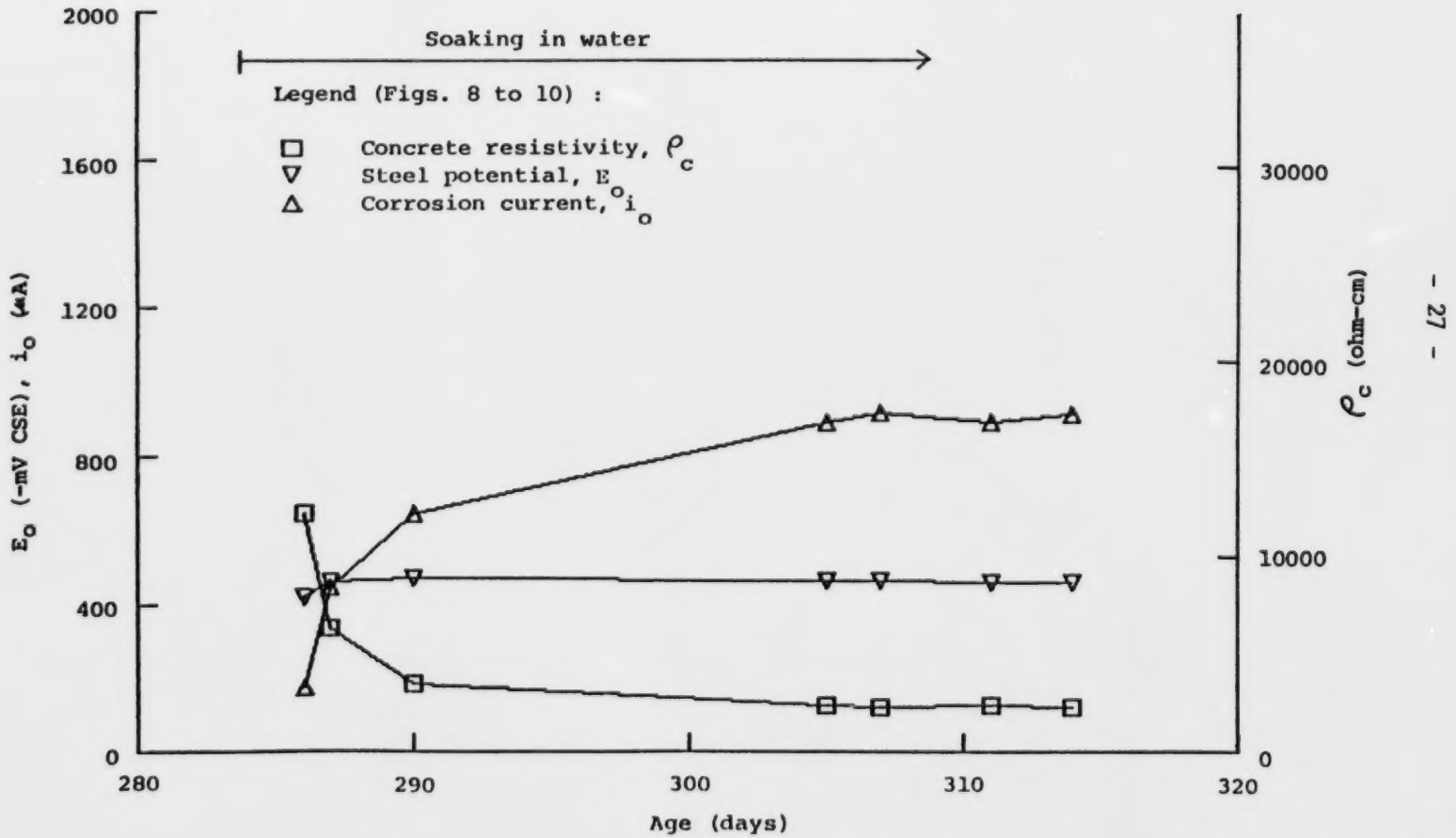

Fig. 8. Average concrete resistivity, steel potential, and corrosion current in the oven dried slabs made with 100 % Portland cement

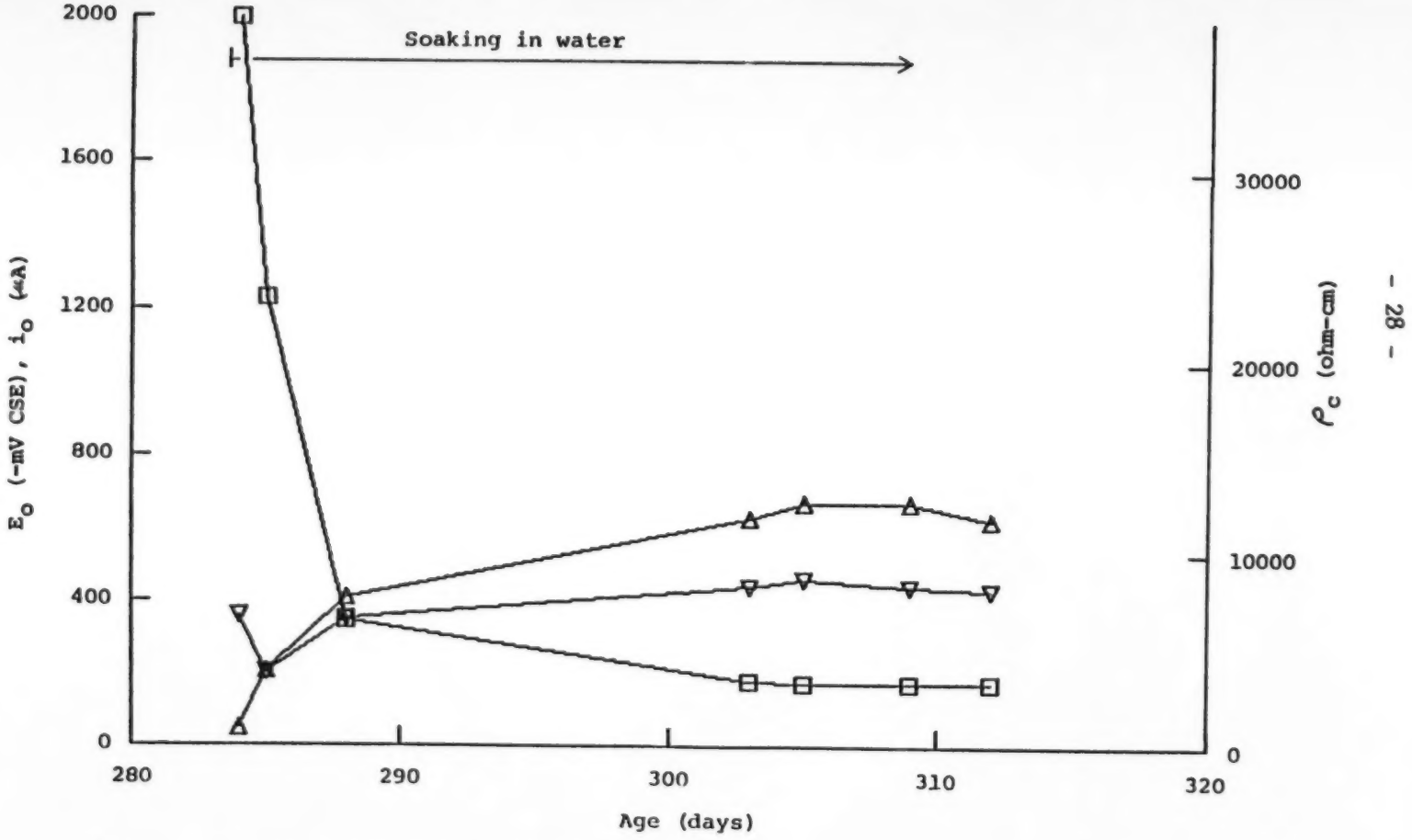

Fig. 9. Average concrete resistivity, steel potential, and corrosion current in the oven dried slabs made with 75 % Portland and 25 % slag cement

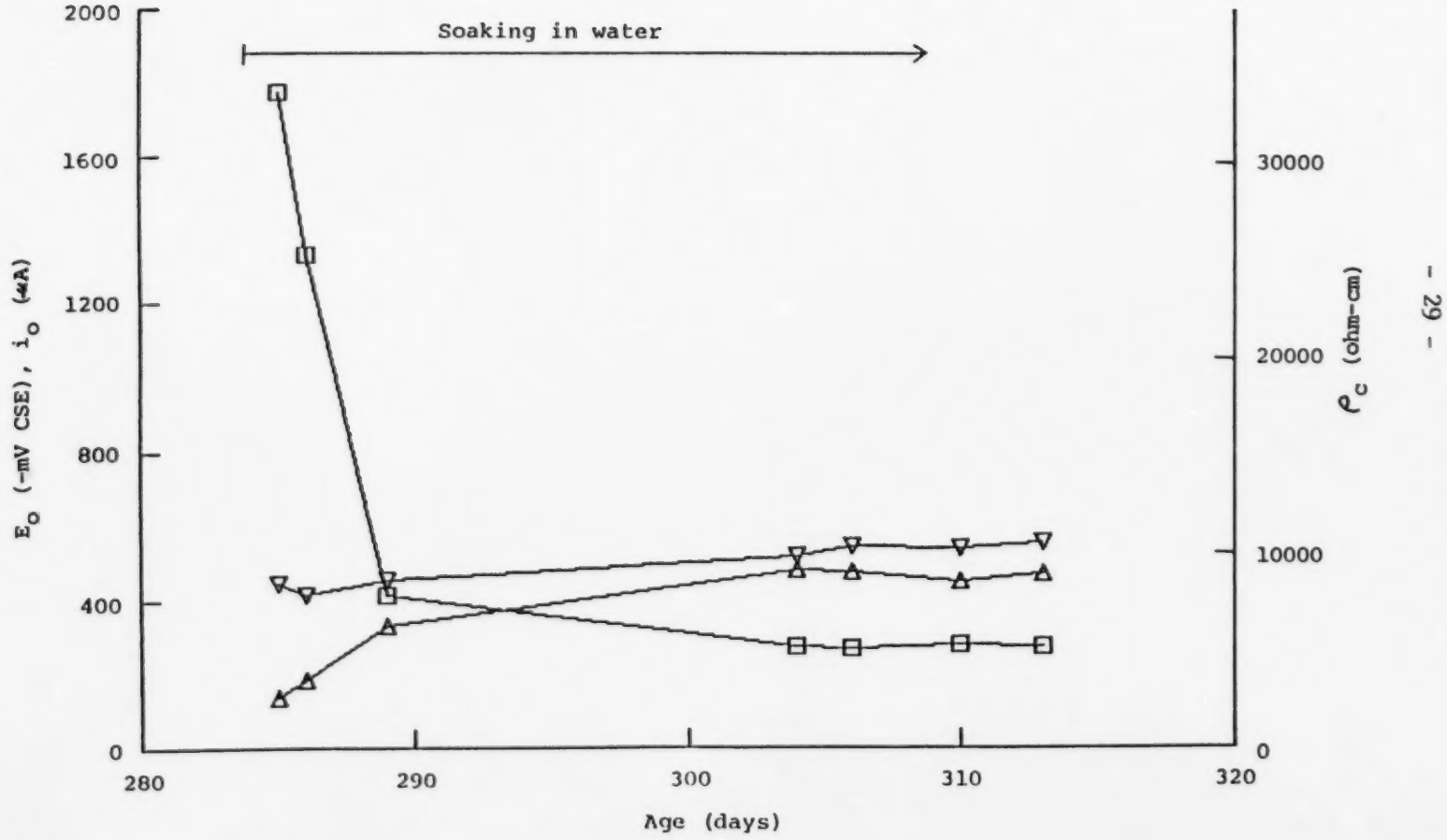

Fig. 10. Average concrete resistivity, steel potential, and corrosion current in the oven dried slabs made with 50 % Portland and 50 % slag cement

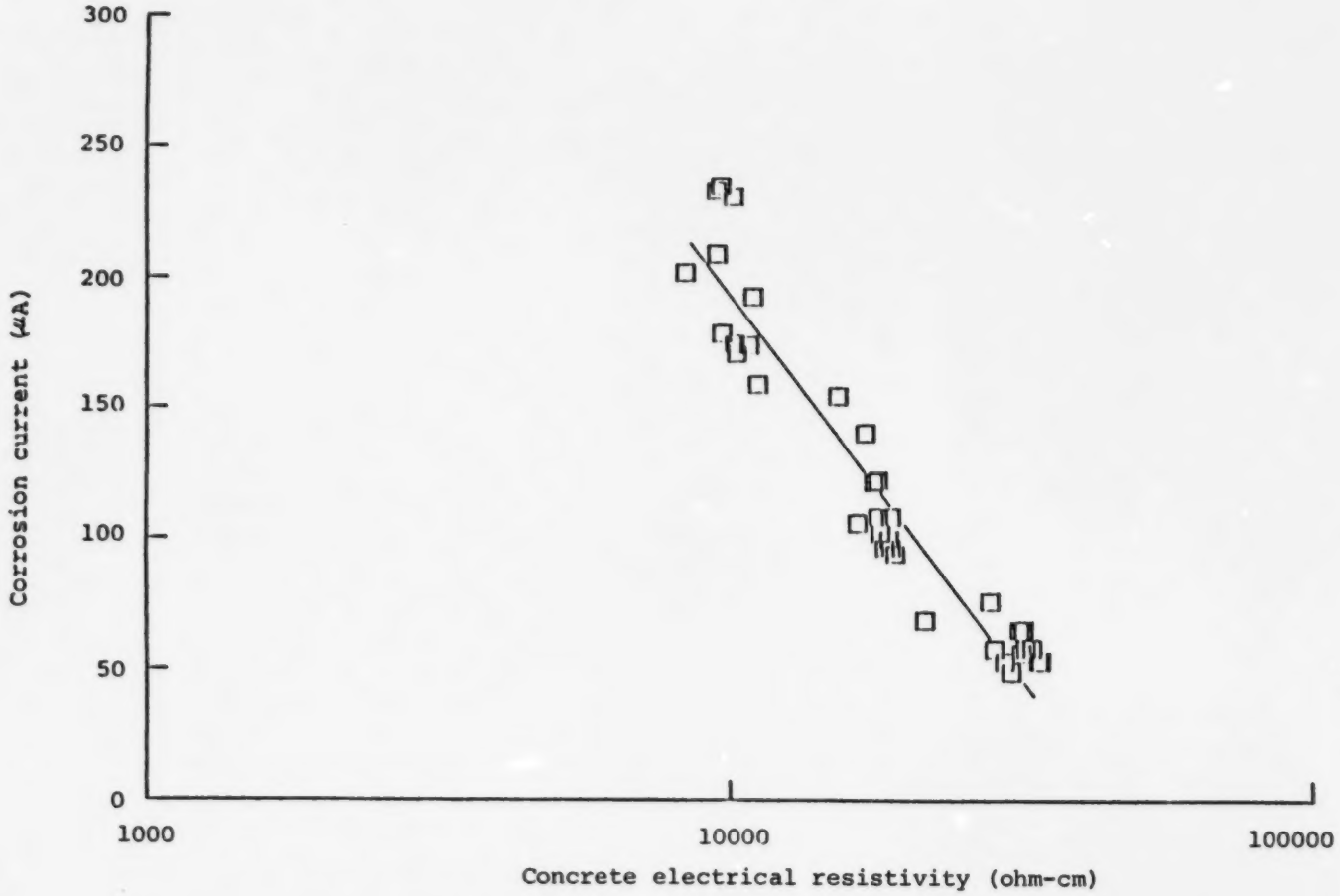

Fig. 11. Relationship between corrosion rate and concrete electrical resistivity

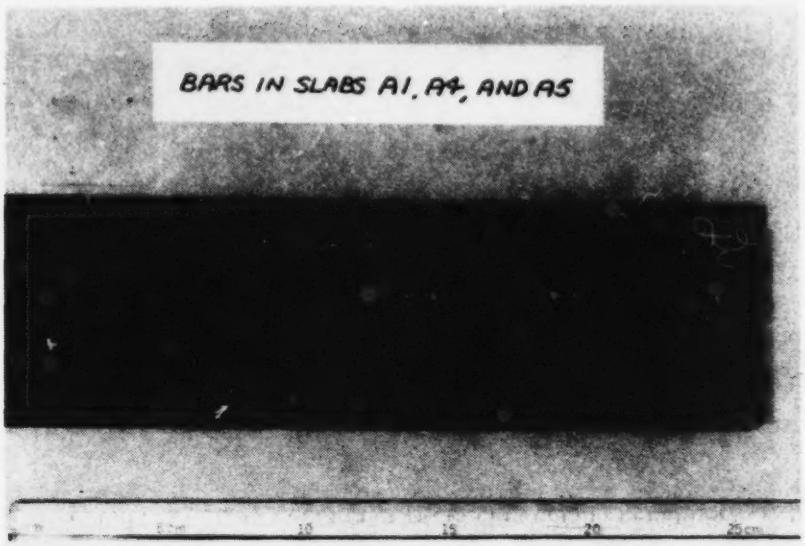

Fig. 12. Corrosion on typical bars embedded in the slabs made with 100 % Portland cement (the bottom four bars were in the oven dried slabs)

Fig. 13. Corrosion on typical bars embedded in the slabs made with 75 % Portland and 25 % slag cement (the bottom four bars were in the oven dried slabs)

Fig. 14. Corrosion on typical bars embedded in the slabs made with 50 % Portland and 50 % slag cement (the bottom four bars were in the oven dried slabs)

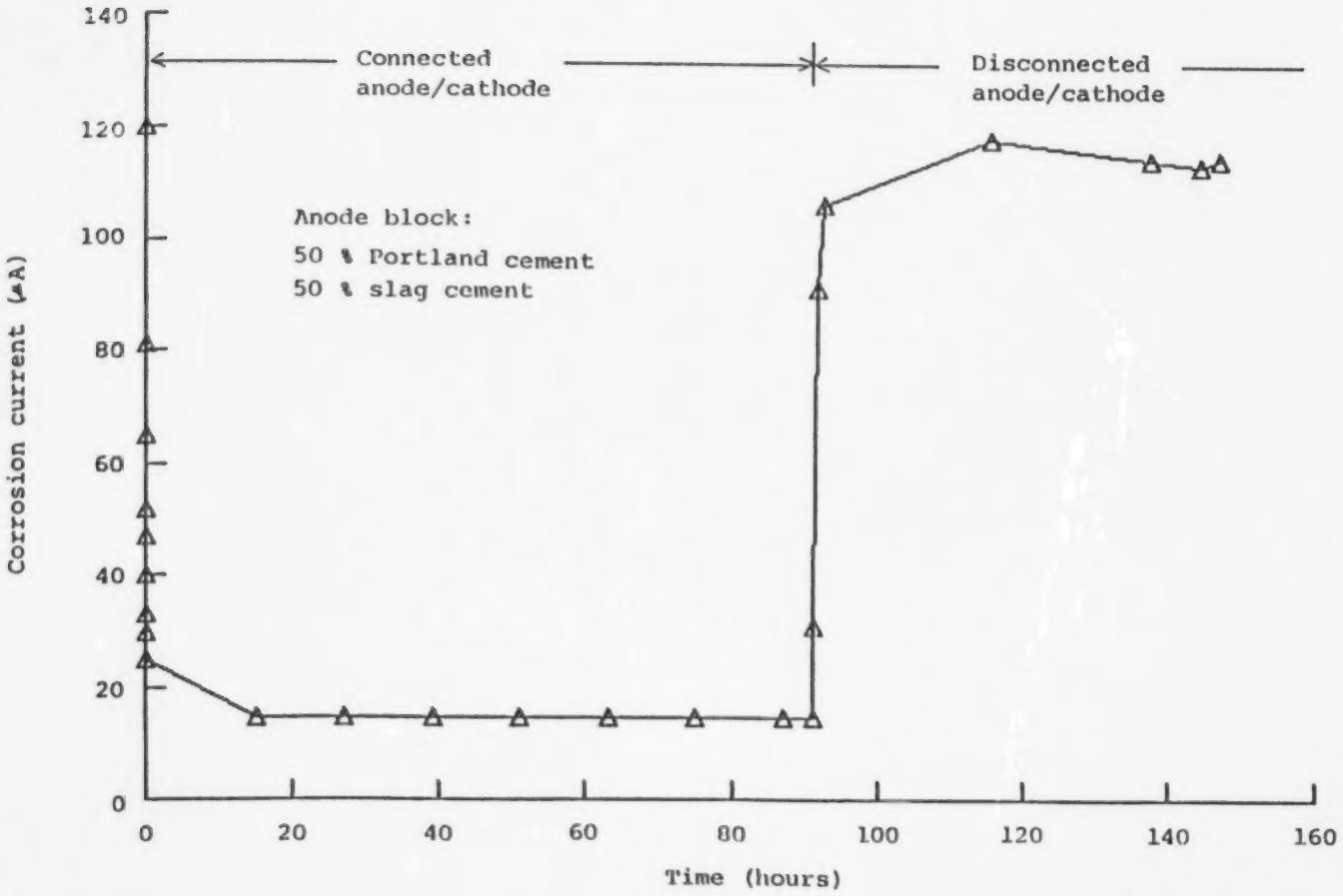

Fig. 15. Macrocell corrosion current in a typical mortared slab

Appendix

Units:

Age	days
Time	hours
δE	mV
R_c	ohms
E_0	-mV, CSE
i_0	μA

Abbreviations:

S	storage condition
1	curing in water
2	1-hour daily ponding with a 3.5% NaCl solution
3	1-day soaking in a 3.5 % NaCl solution and 1-day drying in laboratory air
4	3-day soaking in a 3.5 % NaCl solution and 3-day drying in laboratory air
5	3-day soaking in a 3.5 % NaCl solution and 11-day drying in laboratory air

A.1 Test data for slabs A1, B1 and C1

A.1.1 Slab A1

Age	S	R_c	E_0	i_0
7	1	–	509	456
13	1	244	532	410
14	1	321	501	358
15	1	326	456	397
16	1	323	450	408
20	1	364	222	369
21	1	351	204	358
22	1	341	173	293
23	1	355	153	317
26	1	375	129	305
27	1	359	117	349
28	1	378	121	333
29	1	379	108	298
30	1	379	107	326
33	1	397	102	320
34	1	411	99	301
35	1	421	95	290
36	1	410	87	304
37	2	428	168	288
40	2	536	141	266
41	2	459	187	267
42	2	442	193	310
43	2	436	146	312
44	2	481	148	288
47	2	544	132	233
48	2	522	156	253
49	2	509	162	258
50	2	471	170	275
51	2	476	180	265
54	2	517	170	258
55	2	488	181	244
56	2	497	185	258
57	2	535	186	218
58	2	511	188	245
61	2	550	180	224
62	2	546	189	224
63	2	555	187	217
64	2	554	187	224
68	2	541	191	251
69	3	502	182	210
70	3	541	178	224
72	3	512	176	224
75	3	589	170	186
76	3	547	178	190
78	3	515	177	184
79	3	548	179	204
82	3	520	186	198
84	3	559	172	156
85	3	565	177	197
89	4	493	163	183
90	4	544	169	197

91	4	559	175	197
92	4	565	172	197
96	4	488	367	183
97	4	567	305	177
98	4	565	285	183
99	4	567	291	183
103	4	527	261	167
104	4	554	257	181
105	4	546	258	193
106	4	547	258	197
107	4	519	267	174
109	4	479	254	156
110	4	536	262	152
111	4	567	280	158
112	4	598	271	164
113	4	573	280	176
117	5	436	420	206
118	5	464	415	211
121	5	578	396	185
124	5	574	401	190
125	5	567	397	190
126	5	559	396	199
127	5	548	395	204
128	5	560	394	191
130	5	539	372	156
131	5	441	391	178
132	5	564	395	171
133	5	540	400	175
134	5	582	393	170
138	5	587	380	183
139	5	596	365	168
140	5	602	368	177
141	5	603	354	157
142	5	697	369	145
145	5	612	348	132
146	5	581	354	141
147	5	603	363	99
152	5	585	347	91
153	5	587	364	103
154	5	562	372	115
155	5	510	389	185
156	5	559	374	174
159	5	541	361	198
160	5	550	353	190
163	5	549	359	192
166	5	446	434	191
173	5	541	357	196
175	5	579	335	195
181	5	636	296	171
188	5	586	321	181
194	5	644	298	173

A.1.2 Slab B1

Age	S	R_c	E_0	i_0
7	1	317	194	293
11	1	431	179	267
12	1	466	167	272
13	1	479	153	221
14	1	484	162	238
17	1	–	114	228
18	1	594	156	190
19	1	553	153	190
20	1	560	154	201
21	1	594	154	192
24	1	631	142	171
25	1	631	136	182
26	1	650	134	165
27	1	661	138	177
28	1	669	136	190
31	1	678	127	171
32	1	719	124	149
33	1	732	118	190
34	1	746	119	171
35	2	780	194	152
39	2	821	160	144
40	2	775	194	144
41	2	–	195	157
42	2	773	176	139
45	2	966	142	125
46	2	960	162	127
47	2	890	170	133
48	2	858	170	144
49	2	841	192	134
52	2	908	173	134
53	2	872	184	135
54	2	890	183	136
55	2	947	189	123
56	2	940	188	125
59	2	987	176	122
60	2	971	184	117
61	2	999	184	110
62	2	973	185	112
66	2	975	178	112
67	3	962	185	108
68	3	925	185	115
70	3	925	174	112
73	3	1061	176	103
74	3	1028	185	91
76	3	937	169	89
77	3	1014	179	91
80	3	954	181	94
81	3	1659	162	58
82	3	1030	174	89
83	3	1057	184	90

87	4	1010	289	90
88	4	1037	301	109
89	4	1056	278	91
90	4	1038	275	90
94	4	921	372	90
95	4	1122	359	87
96	4	1092	347	88
97	4	1062	337	90
101	4	1052	333	87
102	4	1109	357	89
103	4	1047	339	92
104	4	1021	344	95
105	4	969	344	93
107	4	916	365	84
108	4	1008	384	76
109	4	1608	387	85
110	4	–	373	82
116	5	972	413	90
119	5	1139	380	84
120	5	927	421	93
121	5	1135	373	85
122	5	1076	369	106
123	5	1066	363	93
124	5	1043	362	90
125	5	1032	362	91
126	5	1035	259	93
128	5	945	361	95
129	5	921	377	85
130	5	1092	394	82
131	5	1058	384	87
132	5	1110	376	85
133	5	1127	372	84
136	5	1125	358	89
137	5	1117	349	83
138	5	1136	344	80
139	5	1139	343	75
140	5	1158	352	72
143	5	1168	379	53
144	5	1102	343	67
145	5	1100	341	57
150	5	1105	409	45
151	5	1062	407	53
152	5	1068	392	50
153	5	993	379	89
154	5	1015	368	85
157	5	984	343	98
158	5	1002	337	98
161	5	1008	335	98
164	5	887	376	92
171	5	1016	302	95
173	5	1077	295	93
179	5	1205	270	84
186	5	1122	263	84
192	5	1233	234	82

A.1.3 Slab C1

Age	S	R_c	E_0	i_0
7	1	261	611	401
12	1	411	607	260
13	1	506	612	228
14	1	540	613	215
15	1	582	604	195
19	1	422	381	163
20	1	751	488	155
21	1	802	428	158
22	1	833	468	141
25	1	977	126	127
26	1	1001	118	117
27	1	977	125	108
28	1	1071	122	114
29	1	1037	112	117
32	1	1165	113	106
33	1	1207	114	100
34	1	1212	109	103
35	1	1268	107	98
36	2	1306	158	90
40	2	1446	170	79
41	2	1377	182	92
42	2	1367	188	92
43	2	1472	143	82
46	2	1671	131	71
47	2	1631	149	71
48	2	1588	143	70
49	2	1532	156	71
50	2	1485	171	73
53	2	1609	166	70
54	2	1544	174	64
55	2	1584	169	67
56	2	1712	167	62
57	2	1611	171	69
60	2	1756	162	64
61	2	1706	165	62
62	2	1743	215	62
63	2	1723	208	64
67	2	1717	176	67
68	3	1536	155	58
69	3	1691	175	62
71	3	1604	177	58
74	3	1765	177	52
75	3	1726	177	54
77	3	1484	178	50
78	3	1752	170	57
83	3	1721	170	50
84	3	1786	164	57
88	4	1561	304	52
89	4	1774	269	53
90	4	1826	265	53

91	4	1832	258	56
95	4	1184	447	61
96	4	1848	352	53
97	4	1823	343	52
98	4	1821	345	54
102	4	–	421	56
103	4	1727	368	53
104	4	1726	350	55
105	4	1710	343	58
106	4	1408	381	53
108	4	1144	422	55
109	4	1167	432	55
110	4	1604	395	52
111	4	1819	358	50
112	4	1753	354	50
116	5	1137	508	65
117	5	1171	393	57
120	5	1929	339	52
124	5	1788	348	58
125	5	1765	350	56
126	5	1761	355	58
127	5	1759	354	58
129	5	1522	359	45
130	5	1327	367	51
132	5	1491	353	59
133	5	1817	351	52
134	5	1885	349	60
137	5	1892	348	50
138	5	1904	342	47
139	5	1897	351	47
140	5	1934	341	45
141	5	1860	356	43
144	5	1900	339	38
145	5	1811	362	42
146	5	1835	652	36
151	5	1481	405	30
153	5	1618	384	35
154	5	1562	375	33
155	5	1534	379	58
156	5	1562	365	56
159	5	1611	352	67
160	5	1748	348	58
163	5	1656	356	60
166	5	1053	602	65
172	5	1658	332	61
174	5	1789	321	62
180	5	1998	290	53
187	5	1841	324	56
193	5	1983	301	52

A.2 Test data for slabs A, B, and C

	Age	S	R_c	E_0	i_0
A2–A6	7	1	296	525	388
	14	1	328	480	370
	21	1	323	193	357
	28	1	381	111	311
	35	1	422	103	278
	42	2	–	–	–
	49	2	514	179	235
	56	2	504	201	234
	62	2	539	208	231
	69	3	505	298	209
	75	3	578	259	193
	84	3	542	257	171
	89	4	513	323	179
	97	4	571	369	174
	112	4	590	343	159
	117	5	445	445	202
	124	5	537	388	175
B2–B6	7	1	324	344	358
	14	1	450	381	260
	21	1	549	259	209
	28	1	627	164	180
	35	2	730	211	157
	42	2	791	176	161
	49	2	808	194	154
	56	2	898	194	140
	62	2	949	188	122
	68	3	932	188	121
	74	3	973	193	96
	83	3	998	246	96
	88	4	958	301	102
	96	4	1010	318	94
	103	4	946	354	108
	111	4	988	353	99
	116	5	874	426	106
	123	5	998	332	108
C2–C6	7	1	230	597	480
	14	1	543	606	212
	21	1	813	283	156
	28	1	1046	121	113
	35	1	1242	112	99
	42	2	1343	204	91
	49	2	1478	185	75
	56	2	1659	196	64
	63	2	1688	201	64
	68	3	1499	198	57
	74	3	1673	203	55
	83	3	1603	211	48
	88	4	1563	241	52
	96	4	1800	335	52
	103	4	1700	344	57
	111	4	1781	341	52
	116	5	1137	483	68
	123	5	1735	342	57

A.3 Test data for the oven dried slabs A, B, and C

	Age	R_c	E_0	i_0
A4-A5	285	-	-	-
	286	645	419	176
	287	339	462	450
	290	184	476	646
	305	130	467	891
	307	125	471	917
	311	126	462	895
	314	125	461	913
B4-B5	283	-	-	-
	284	4562	357	49
	285	1231	200	208
	288	350	355	411
	303	181	444	633
	305	174	461	672
	309	177	440	671
	312	177	431	624
C4-C5	284	-	-	-
	285	1773	449	138
	286	1334	418	185
	289	416	460	334
	304	275	521	485
	306	269	547	481
	310	278	543	454
	313	276	559	475

A.4 Test data for the mortared slabs

A.4.1 Slab A4 (Bar #10)

Time	δE	Time	δE
0.000	6.79	0.590	0.99
0.003	3.64	1.790	0.84
0.021	2.77	2.990	0.80
0.040	1.97	4.190	0.77
0.065	1.74	6.590	0.77
0.096	1.57	8.990	0.77
0.130	1.46	11.40	0.73
0.160	1.37	13.80	0.73
0.190	1.31	16.20	0.73
0.220	1.28	18.60	0.70
0.255	1.21	21.00	0.70
0.284	1.18	23.40	0.70
0.315	1.14	27.00	0.70
0.345	1.12	Disconnected	
0.380	1.10	27.90	5.57
0.410	1.07	37.74	7.69
0.440	1.06	60.74	8.05
0.470	1.04		
0.505	1.03		
0.535	1.01		
0.565	1.00		

A.4.2 Slab B3 (Bar #7)

Time	δE	Time	δE
0.000	5.40	0.405	0.97
0.006	3.35	0.440	0.96
0.019	2.60	0.470	0.94
0.056	1.84	0.500	0.93
0.075	1.67	0.545	0.90
0.100	1.50	13.00	0.73
0.125	1.40	25.00	0.70
0.155	1.30	Disconnected	
0.190	1.20	26.15	3.63
0.220	1.14	26.75	4.23
0.250	1.10	38.65	5.62
0.280	1.09	44.55	5.81
0.315	1.05	62.25	6.14
0.345	1.03		
0.375	0.99		

A.4.3 Slab C4 (Bar #12)

Time	δE	Time	δE
0.000	6.02	51.00	0.73
0.003	4.05	63.00	0.73
0.009	3.23	75.00	0.74
0.022	2.61	87.00	0.74
0.035	2.33	91.00	0.74
0.055	2.00	Disconnected	
0.100	1.60	91.02	1.57
0.160	1.48	92.60	5.32
0.220	1.25	115.25	5.90
15.00	0.73	137.25	5.72
27.00	0.73	144.15	5.65
39.00	0.73	147.00	5.72
51.00	0.73		

A.4.4 Slab C4 (Bar #10)

Time	δE	Time	δE
0.000	6.40	0.690	1.48
0.004	3.73	0.755	1.47
0.011	3.17	0.815	1.46
0.023	2.27	0.880	1.44
0.055	2.37	0.940	1.42
0.075	2.25	1.005	1.41
0.090	2.15	1.070	1.40
0.130	2.00	1.130	1.40
0.160	1.93	1.190	1.40
0.190	1.97	12.15	1.25
0.255	1.90	23.50	1.18
0.285	1.80	29.00	1.15
0.315	1.79	Disconnected	
0.380	1.75	30.00	3.90
0.440	1.57	30.50	5.88
0.505	1.54	45.50	5.90
0.565	1.50	59.00	5.60
0.630	1.49		